A Combined Parameter and Function Estimation Approach for Prediction of Solidification/Melting Process in a Smelting Furnace

Vahid Tahmasbi [a], Seyed Mohammad Hossein Karimian [b,*], Sahar Noori [b]

[a] Aerospace Research Institute, Amirkabir University of Technology (Tehran Polytechnic), Tehran, Iran

[b] Department of Aerospace Engineering, Amirkabir University of Technology (Tehran Polytechnic), Tehran, Iran

Address correspondence to Seyed Mohammad Hossein Karimian, Department of Aerospace Engineering, Amirkabir University of Technology (Tehran Polytechnic), No. 350, Hafez Ave, Valiasr Square, Tehran, Iran 1591634311. E-mail: hkarim@aut.ac.ir

Abstract

In a high-temperature smelting furnace, the bank layer acts as a barrier to protect the brick wall against the highly corrosive liquid slag. The present contribution proposes an inverse heat conduction method as a simultaneous parameter and function estimation approach to precisely predict the time-varying bank thickness. The crucial parameters that affect the bank formation include the thermal conductivity of both slag and refractory brick wall, and the heat transfer coefficient between the external wall of the furnace and the surrounding environment. These parameters, as well as the time-varying heat load of the furnace, constitute the unknowns of the inverse solution. The enthalpy method is adopted to simulate the phase change process. The sensitivity and adjoint equations for a furnace with non-constant density Phase Change Material are derived for the first time in the present study. The verification of the proposed hybrid method has been performed via several simulated experiments. The results for the case with errorless measurement showed that the error of the solid front is within the range of approximately ±2%.

* Corresponding author. Tel: +98 21 64543206 E-mail addresses: hkarim@aut.ac.ir

Introduction

A smelting furnace is a device employed to melt materials, such as steel and copper, requiring high energy and temperature. The required energy to melt material is provided using high voltage electrodes embedded in these furnaces. The resulting electric power is converted into thermal energy based on the Joule heating phenomenon and transferred through the slag/metal interface [1-3]. Due to the high latent heat of fusion of the slag substance, it is classified as solid-liquid Phase Change Material (PCM). The molten PCM is cooled upon contact with the brick wall, forming a solid layer called a “bank”. The bank protects the brick wall against the highly corrosive liquid slag. The components of a smelting furnace are depicted schematically in Fig. 1.

The smelting furnace should be designed so that the thickness of the bank formed on the slag/brick interface does not decrease below a certain threshold. On the other hand, increasing the bank thickness reduces the amount of liquid slag required for the smelting process [1]. Preserving the bank thickness in the desired range is usually done by controlling the heat flux applied to the furnace [1].

One way to determine the bank thickness is to measure it during the furnace operation. However, due to complex phenomena in the slag region, such as flow circulation, the measured thickness by submerged probes is usually not reliable [2]. Among the methods proposed for modeling the solid-liquid phase change phenomenon, the so-called enthalpy method is prevalent due to its simplicity and high efficiency [3]. Accordingly, for non-eutectic alloys or impure materials, a mushy zone (i.e., mutual existence of solid and liquid phases) appears over an extended temperature range [4]. In contrast to the so-called adaptive methods [5], the single region formulation of the melting-

solidification process in the enthalpy method removes the need to track the moving solid-liquid interface.

In order to use the enthalpy method (or adaptive ones) for simulation of the solidification-melting process in a furnace, the energy transferred from the electrodes to the slag bath must be known in advance. The heat transfer process from the arc to the slag region is carried out by various mechanisms, i.e., radiation, convection, condensation, and energy transported by electrons [6]. Therefore, many partial differential equations must be solved simultaneously to predict the transient behavior of the slag and, consequently, the bank formation inside the furnace. This process can be very complicated and time-consuming. This shortcoming can be resolved by inverse heat transfer techniques that have attracted much attention in the last decade [1-3, 7-19].

An inverse heat transfer problem is used to estimate the unknown causal parameter from the given temperatures recorded by the thermocouples embedded inside the medium [20, 21]. The inverse heat transfer methods have been successfully applied to predict the thermal properties and boundary conditions of PCMs [22-24]. A common strategy for predicting the bank thickness in a smelting furnace by an inverse method involves the following basic steps [17]:

i) The sensor(s) are installed inside the refractory brick material to measure temperature.

ii) The temperature measurements are used in an inverse process to estimate the heat flux applied to the slag region.

iii) The estimated heat flux is used as the boundary condition of the direct model, and the bank thickness is predicted.

Tadrari and Lacroix [1] employed Conjugate Gradient Method (CGM) with the adjoint problem to estimate the time-varying heat flux applied to the slag region. They showed that the proposed

method is stable and accurate enough, even in the case of noisy measurements. Marois et al. [9, 25] addressed the bank formation in PCMs with large thermal inertia. The main problem encountered in their work was the significant time delay of the in-depth temperature response to the applied heat flux (or solidification front location). In another study [10], they proposed a two-dimensional inverse heat transfer method for predicting the shape of the bank in a smelting furnace. Since the proposed minimization algorithm relied on the Levenberg Marquardt Method (LMM) [26] and finite difference approximation of the Jacobian matrix, the computations were not efficient in terms of time-consuming. To eliminate this drawback, LeBreux et al. [11-13] examined the capability of the Kalman filter method [8] in predicting bank thickness in metallurgical reactors.

The abovementioned studies considered the time-varying lateral heat flux as the only unknown in their inverse solution. Therefore, any uncertainty in the thermal properties can become an important source of error in the estimated heat flux and, consequently, bank thickness. In order to attenuate the uncertainty error, simultaneous estimation of the heat flux and thermal properties has recently been the subject of a few investigations [15, 17-19]. In Hafid and Lacroix's studies [15, 17, 18], a one-dimensional inverse heat transfer method was utilized to simultaneously estimate the boundary heat flux and thermophysical properties of both molten material and refractory brick wall. The unknown thermophysical properties in their work included external heat transfer coefficient [17], the thermal conductivity of PCM and brick wall [15], and thermal contact resistance between the protective bank and inner lining of the refractory brick wall [18]. Later, in a more comprehensive study, Zhang et al. [19] proposed a two-dimensional transient inverse model to predict the bank shape varied temporally and spatially.

Inverse problems can conventionally be considered either as a parameter or as a function estimation approach [27-34]. Some works have solved the problem in the form of simultaneous parameter and function estimation [35]. The common point of all reviewed articles [15, 17-19] was that the inverse problem was solved as a parameter estimation approach. In fact, their inverse process required some prior information regarding the functional form of the heat flux. Although applying this assumption (parameterizing the heat flux function) makes it easier to solve the inverse problem, it does not necessarily correspond to the actual condition in the furnace. Overcoming this drawback is the main subject of the present contribution.

The present study is devoted to developing a combined parameter and function estimation approach for accurately predicting the thickness of the bank formed on the inner lining of the refractory brick wall in a smelting furnace. The unknown function to be estimated is the time-varying heat load of the furnace without any prior knowledge on its functional form. So, the unknown heat flux function is considered in an infinite-dimensional form [36-39], where the heat flux function is estimated at grid points of the time frame. The vector of unknown parameters contains are the thermal conductivity of the solid PCM (bank layer), the thermal conductivity of the refractory brick wall, and the heat transfer coefficient between the external wall of the furnace and surrounding environment. The phase change process during the slag solidification is modeled by the enthalpy method. Unlike the previous source-based models [18] that assumed a constant density for PCM, the current conservative formulation makes it possible to consider different density values for the liquid and solid states. With this assumption, direct, sensitivity, and adjoint equations are constructed. It is worth noting that the sensitivity and adjoint equations for a furnace with non-constant PCM density are derived for the *first time* in the present study.

Physical model and assumptions

The physical problem consists of the slag bath and refractory brick wall of thicknesses d_{pcm} and d_{brick}, respectively. The geometry of this problem is depicted in Fig. 2. The left surface of the PCM is exposed to a transient heat flux of $q(t)$, and the ambient air with a temperature of T_∞ cools the outer surface of the brick wall with a heat transfer coefficient of h_∞. The PCM in the slag bath is in the liquid, mushy and solid phases. The brick wall is protected against corrosion by the solid layer (bank) of thickness $\delta(t)$. The thermocouple(s) are placed inside the brick wall region at a depth of x_m from the exposed surface of the slag.

The following assumptions are considered to obtain a mathematical model.

1. The thermophysical properties of the PCM, including density, thermal conductivity, and heat capacity, are assumed to be constant in solid and liquid states. The values of these properties in the mushy zone vary linearly between the values of the solid and liquid states.
2. The thermophysical properties of bricks are assumed to be constant.
3. Thermal contact resistance between the brick wall and the slag is neglected.
4. The temperature gradient in the vertical direction is negligible compared to the lateral direction, so a one-dimensional mathematical model for heat transfer has been selected.
5. The phase change from solid to liquid (and vice versa) is considered non-isothermal.
6. The flow circulation in the slag bath is not modeled. Therefore, the heat transfer mechanism in the liquid slag is assumed to be conduction dominant [40]. The effect of flow circulation can be compensated by selecting an empirically thermal conductivity coefficient higher than the nominal value in the liquid phase [1].

Direct problem

The well-posed direct problem is defined as determining the temperature distribution inside the PCM and the brick wall from the given time-varying heat flux and thermal properties of the furnace. According to the assumptions outlined in section 2, the mathematical formulation of the direct problem is given by:

For the PCM (slag):

$$\frac{\partial}{\partial t}\left(\rho_1 Cp_1 T_1 + f\,\rho_1 L\right) - \frac{\partial}{\partial x}\left(k_1 \frac{\partial T_1}{\partial x}\right) = 0; \quad 0 < x < d_{pcm} \text{ and } 0 < t \le t_f \tag{1a}$$

$$k_1 \frac{\partial T_1}{\partial x} = -q(t); \quad x = 0 \text{ and } 0 < t \le t_f \tag{1b}$$

$$T_1(x,0) = T_{01}(x); \quad 0 < x < d_{pcm} \text{ and } t = 0 \tag{1c}$$

where

$$f(T_1) = \begin{cases} 1; & T_S \ge T_1 \\ \dfrac{T_1 - T_S}{T_L - T_S}; & T_S < T_1 < T_L \\ 0; & T_L \le T_1 \end{cases} \tag{1d}$$

$$k_1 = f k_L + (1-f)\,k_S \tag{1e}$$

$$\rho_1 = f\,\rho_L + (1-f)\,\rho_S \tag{1f}$$

$$\rho_1 Cp_1 = f\,\rho_L Cp_L + (1-f)\,\rho_S Cp_S \tag{1g}$$

For the brick wall:

$$\rho_2 Cp_2 \frac{\partial T_2}{\partial t} - k_2 \frac{\partial^2 T_2}{\partial x^2} = 0; \quad d_{pcm} < x < d_{pcm} + d_{brick} \text{ and } 0 < t \le t_f \tag{2a}$$

$$k_2 \frac{\partial T_2}{\partial x} = h_\infty \left(T_\infty - T_2 \right); \quad x = \left(d_{pcm} + d_{brick} \right) \; and \; 0 < t \le t_f \tag{2b}$$

$$T_2 \left(x, 0 \right) = T_{02}(x); \quad d_{pcm} < x < d_{pcm} + d_{brick} \; and \; t = 0 \tag{2c}$$

At the brick-slag interface:

$$k_1 \frac{\partial T_1}{\partial x} = k_2 \frac{\partial T_2}{\partial x}; \quad x = d_{pcm} \; and \; 0 < t \le t_f \tag{3a}$$

where

$$T_1 \left(d_{pcm}, t \right) = T_2 \left(d_{pcm}, t \right) \tag{3b}$$

It should be noted that if the liquid and solid density of the PCM are considered to be the same ($\rho_L = \rho_S$), Eq. (1a) is reduced to that presented by previous works [15, 16]. The finite volume fully implicit approach is used to discretize the direct equations. The resulting non-linear system of equations is solved by the Newton-Raphson method.

Direct code verification

The numerical and semianalytical results of Voller and Swaminathan [41] are used to verify the developed model. Voller and Swaminathan [41] studied the solidification of a binary Al-4.5% Cu alloy. The properties of the PCM material used by Voller and Swaminathan [41] are summarized in Table 1. The left boundary of their sample with a thickness of 0.5 m was kept at a constant temperature of 573 K, and the right boundary was adiabatic. The initial temperature of the sample was set to be 969 K. The time step of 2s and the grid size of 0.005 m are employed in the numerical simulation. Figure 3 compares the predicted location of the solidus and liquidus fronts by the present model versus those reported by Voller and Swaminathan [41]. According to this figure, the maximum discrepancy between the results appears at later times. Accordingly, the

maximum deviation of the present enthalpy method from the semi-analytical heat balance approach and the numerical source-based method of Voller and Swaminathan [41] is 7.9% and 1.7% for the liquidus front, and 6.9% and 4.2% for the solidus front. The discrepancies between the present results and those obtained by Voller and Swaminathan can be attributed to the different methods used to model the heat of fusion.

Inverse problem

An inverse problem is characterized by estimating the unknown causes from the given effects. In the current inverse heat conduction problem, the unknowns are time-varying heat flux $q(t)$, the external heat transfer coefficient h_∞, the thermal conductivity of the solid PCM k_S and thermal conductivity of the brick wall k_2. The simultaneous estimation of heat flux function and thermophysical parameters improves the inverse method in terms of uniqueness of the solution. The simulated temperature measurements of sensors are obtained by the solution of the direct problem as outlined in section 3. If the temperature data acquired by the sensors can be approximated as a continuous function, the solution of the current inverse problem is achieved by minimizing the following objective function:

$$S[\boldsymbol{P}] = \sum_{m=1}^{M} \int_{t=0}^{t_f} \left[Y_m(t) - T_2(x_m, t; \boldsymbol{P}) \right] \tag{4}$$

In this equation, $Y_m(t)$ and $T_2(x_m, t; \boldsymbol{P})$ represent, respectively, the measured and simulated temperatures at the sensor location x_m. The unknowns in the present inversion are assembled in a single vector $\boldsymbol{P}$ as follows:

$$\boldsymbol{P}^T = [h_\infty, k_S, k_2, q_0, q_1, q_2, ..., q_N] \tag{5}$$

where $q_j; j = 0,1,2,...,N$ are the components of the heat flux at a time $t_j; j = 0,1,2,...,N$. The total time of the problem is divided into *N* equal segments and q_j are heat fluxes at boundary points of these time segments. Therefore, the function of heat flux *q(t)* in terms of its components q_j can be expressed as follows:

$$q(t) = \sum_{j=1}^{N} q_j B_j(t) \tag{6}$$

where $B_j(t)$ are the known B-spline functions on time. If *N* equals the total time steps of the direct problem, then the heat flux function *q(t)* is estimated at each time step, and the B-Spline function is no longer required $\left[q(t_j) = q_j; j = 0,1,2,...,N \right]$. In the current estimation, the heat flux components are represented at grid points, typically called ***infinite-dimensional form*** [38].

Minimization procedure

A well-known gradient-based algorithm for solving non-linear inverse problems, i.e., the Conjugate Gradient Method, is adopted in this study. The iterative procedure of CGM for minimization of the objective function $S[\boldsymbol{P}]$ (Eq. (4)) is given in the form:

$$q^{i+1}(t) = q^{i}(t) - \beta_q^i d_q^i(t) \tag{7a}$$

$$\begin{bmatrix} h_\infty \\ k_S \\ k_2 \end{bmatrix}^{i+1} = \begin{bmatrix} h_\infty \\ k_S \\ k_2 \end{bmatrix}^{i} - \begin{bmatrix} \beta_{h_\infty} d_{h_\infty} \\ \beta_{k_S} d_{k_S} \\ \beta_{k_2} d_{k_2} \end{bmatrix}^{i+1} \tag{7b}$$

where $d_q^i(t)$ is the directions of descent for the heat flux, d_{h_∞}, d_{k_S} and d_{k_2} are, respectively, the directions of descent for the external heat transfer coefficient, the thermal conductivity of the solid PCM and of the brick wall, β are the values of the search step size and the superscript *i*

represents the iteration number. In CGM, the direction of descent is obtained by conjugation of the gradient vector and the previous direction of descent as follows:

$$d_q^i = \nabla S\left[q^i(t)\right] + \gamma_q^i d_q^{i-1}(t) \tag{8a}$$

$$\begin{bmatrix} d_{h_\infty} \\ d_{k_S} \\ d_{k_2} \end{bmatrix}^i = \begin{bmatrix} \nabla S(h_\infty) \\ \nabla S(k_S) \\ \nabla S(k_2) \end{bmatrix}^i + \begin{bmatrix} \gamma_{h_\infty} d_{h_\infty} \\ \gamma_{k_S} d_{k_S} \\ \gamma_{k_2} d_{k_2} \end{bmatrix}^{i-1} \tag{8b}$$

The conjugation coefficients γ_q^i, $\gamma_{h_\infty}^i$, γ_{k_S} and γ_{k_2} are computed based on the Polak-Ribiere [38] expression as:

$$\gamma_q^i = \frac{\int_{t=0}^{t_f} \left\{\nabla S\left[q^i(t)\right] - \nabla S\left[q^{i-1}(t)\right]\right\} \nabla S\left[q^i(t)\right] dt}{\int_{t=0}^{t_f} \left\{\nabla S\left[q^{i-1}(t)\right]\right\}^2 dt} \tag{9a}$$

$$\gamma_{h_\infty}^i = \frac{\nabla S\left(h_\infty^i\right)\left[\nabla S\left(h_\infty^i\right) - \nabla S\left(h_\infty^{i-1}\right)\right]}{\left[\nabla S\left(k_S^{i-1}\right)\right]^2 + \left[\nabla S\left(k_2^{i-1}\right)\right]^2 + \left[\nabla S\left(h_\infty^{i-1}\right)\right]^2} \tag{9b}$$

$$\gamma_{k_S}^i = \frac{\nabla S\left(k_S^i\right)\left[\nabla S\left(k_S^i\right) - \nabla S\left(k_S^{i-1}\right)\right]}{\left[\nabla S\left(k_S^{i-1}\right)\right]^2 + \left[\nabla S\left(k_2^{i-1}\right)\right]^2 + \left[\nabla S\left(h_\infty^{i-1}\right)\right]^2} \tag{9c}$$

$$\gamma_{k_2}^i = \frac{\nabla S\left(k_2^i\right)\left[\nabla S\left(k_2^i\right) - \nabla S\left(k_2^{i-1}\right)\right]}{\left[\nabla S\left(k_S^{i-1}\right)\right]^2 + \left[\nabla S\left(k_2^{i-1}\right)\right]^2 + \left[\nabla S\left(h_\infty^{i-1}\right)\right]^2} \tag{9d}$$

Sensitivity problem and search step size

The sensitivity temperature functions $\Delta T_1(x,t)$ and $\Delta T_2(x,t)$ are defined as the change in temperature due to perturbation of the unknown parameters or function. Directional perturbation of the heat flux components causes directional changes in sensors' temperature, obtained by

solving the sensitivity problem. If the heat flux function *q(t)* is perturbed by an amount of $\varepsilon\Delta q(t)$, the temperature functions $T_1(x,t)$ and $T_2(x,t)$ and liquid fraction $f(T_1)$ undergo the following variations:

$$T_{1\varepsilon}(x,t) = T_1(x,t) + \varepsilon\Delta T_1(x,t) \tag{10a}$$

$$T_{2\varepsilon}(x,t) = T_2(x,t) + \varepsilon\Delta T_2(x,t) \tag{10b}$$

$$f_\varepsilon(T_{1\varepsilon}) = f(T_{1\varepsilon}) + \varepsilon\frac{\partial f}{\partial T_1}\Delta T_1(x,t) \tag{10c}$$

where

$$\lambda(T_1) \equiv \frac{\partial f}{\partial T_1} = \begin{cases} 1; & T_S \geq T_1 \\ \dfrac{1}{T_L - T_S}; & T_S < T_1 < T_L \\ 0; & T_L \leq T_1 \end{cases} \tag{10d}$$

If $D_1(T_1)=0$ and $D_2(T_2)=0$ represent the direct equations for the slag and brick wall, respectively; the sensitivity problem is obtained by applying the following limiting processes:

$$\lim_{\varepsilon\to 0}\frac{D_{\varepsilon 1}(T_{1\varepsilon}) - D_1(T_1)}{\varepsilon} = 0 \tag{11a}$$

$$\lim_{\varepsilon\to 0}\frac{D_{\varepsilon 2}(T_{2\varepsilon}) - D_2(T_2)}{\varepsilon} = 0 \tag{11b}$$

Applying the above limiting processes to the direct equations and their initial and boundary conditions, and after some manipulations, the following sensitivity problems are obtained for the determination of the temperature sensitivity functions $\Delta T_1(x,t)$ and $\Delta T_2(x,t)$.

For the slag bath:

$$\frac{\partial \bar{C} T_1}{\partial t} - \frac{\partial^2 \left(k_1 \Delta T_1\right)}{\partial x^2} = 0; \quad 0 < x < d_{pcm} \; and \; 0 < t \le t_f \tag{12a}$$

$$\frac{\partial \left(k_1 \Delta T_1\right)}{\partial x} = -\Delta q(t); \quad x = 0 \; and \; 0 < t \le t_f \tag{12b}$$

$$\Delta T_1(x,0) = 0; \quad 0 < x < d_{pcm} \; and \; t = 0 \tag{12c}$$

where

$$\bar{C} = \rho_1 Cp_1 + T_1 \lambda(T_1)\left[\rho_L Cp_L - \rho_S Cp_S\right] + L\lambda(T_1)\left[\rho_1 + f\left(\rho_L - \rho_S\right)\right] \tag{12d}$$

For the brick wall:

$$\rho_2 Cp_2 \frac{\partial \Delta T_2}{\partial t} - k_2 \frac{\partial^2 \Delta T_2}{\partial x^2} = 0; \quad d_{pcm} < x < d_{pcm} + d_{brick} \; and \; 0 < t \le t_f \tag{13a}$$

$$k_2 \frac{\partial \Delta T_2}{\partial x} = -h_\infty \Delta T_2; \quad x = \left(d_{pcm} + d_{brick}\right) and \; 0 < t \le t_f \tag{13b}$$

$$\Delta T_2(x,0) = 0; \quad d_{pcm} < x < d_{pcm} + d_{brick} \; and \; t = 0 \tag{13c}$$

At the brick-slag interface:

$$\frac{\partial \left(k_1 \Delta T_1\right)}{\partial x} = k_2 \frac{\partial \Delta T_2}{\partial x}; \quad x = d_{pcm} \; and \; 0 < t \le t_f \tag{14a}$$

where

$$\Delta T_1\left(d_{pcm}, t\right) = \Delta T_2\left(d_{pcm}, t\right) \tag{14b}$$

Calculation of the sensitivity function for the thermal conductivity and external heat transfer coefficient is performed using a Jacobian matrix defined by the first-order partial derivatives of the temperatures with respect to the unknown parameters, as follows:

$$\boldsymbol{J}=\begin{bmatrix} \dfrac{\partial T_{21}}{\partial h_\infty} & \dfrac{\partial T_{21}}{\partial k_S} & \dfrac{\partial T_{21}}{\partial k_2} \\ \dfrac{\partial T_{22}}{\partial h_\infty} & \dfrac{\partial T_{22}}{\partial k_S} & \dfrac{\partial T_{22}}{\partial k_2} \\ \vdots & \vdots & \vdots \\ \dfrac{\partial T_{2I}}{\partial h_\infty} & \dfrac{\partial T_{2I}}{\partial k_S} & \dfrac{\partial T_{2I}}{\partial k_2} \end{bmatrix} \tag{15}$$

where *I* refer to the total number of measurements. Finite difference approximation is used for determining the components of Jacobian matrix, ***J***, as follows:

$$J_{i1}=\frac{\partial T_{2i}}{\partial h_\infty}=\frac{T_{2i}\left(\boldsymbol{q},h_\infty+\varepsilon h_\infty,k_S,k_2\right)-T_{2i}\left(\boldsymbol{q},h_\infty,k_S,k_2\right)}{\varepsilon h_\infty}+o\left(\varepsilon h_\infty\right) \tag{16a}$$

$$J_{i2}=\frac{\partial T_{2i}}{\partial k_S}=\frac{T_{2i}\left(\boldsymbol{q},h_\infty,k_S+\varepsilon k_S,k_2\right)-T_{2i}\left(\boldsymbol{q},h_\infty,k_S,k_2\right)}{\varepsilon k_S}+o\left(\varepsilon k_S\right) \tag{16b}$$

$$J_{i3}=\frac{\partial T_{2i}}{\partial k_2}=\frac{T_{2i}\left(\boldsymbol{q},h_\infty,k_S,k_2+\varepsilon k_2\right)-T_{2i}\left(\boldsymbol{q},h_\infty,k_S,k_2\right)}{\varepsilon k_2}+o\left(\varepsilon k_2\right) \tag{16c}$$

where $\varepsilon=10^{-3}$ is chosen in the current study.

The search step sizes β_q^i and β_k^i in Eqs. (7) are calculated by minimizing the objective function *S[**P**]* (see Eq. (4)) with respect to β_q^i and β_k^i, that is:

$$\min_{\beta_q^i \text{ and } \beta_k^i} S\left[\boldsymbol{q}^{i+1},\boldsymbol{k}^{i+1}\right]=\min_{\beta_q^i \text{ and } \beta_k^i}\sum_{m=1}^{M}\int_{t=0}^{t_f}\left[Y_m\left(t\right)-T_{2m}\left(\boldsymbol{q}^i-\beta_q^i\boldsymbol{d}_q^i,\boldsymbol{k}^i-\beta_{h_\infty}^i d_{h_\infty}^i-\beta_{k_S}^i d_{k_S}^i-\beta_{k_2}^i d_{k_2}^i\right)\right]^2 dt \tag{17}$$

where $\boldsymbol{q}^T\equiv\left[q_j;\,j=1,...,N\right]$, $\boldsymbol{k}^T\equiv\left[h_\infty,k_S,k_2\right]$ and $\boldsymbol{d}_q^T\equiv\left[d_{qj};\,j=1,...,N\right]$. The temperature T_{2m} is approximated by the Taylor series expansion as follows:

$$T_{2m}\left(\boldsymbol{q}^i-\beta_q^i\boldsymbol{d}_q^i,\boldsymbol{k}^i-\beta_{h_\infty}^i d_{h_\infty}^i-\beta_{k_S}^i d_{k_S}^i-\beta_{k_2}^i d_{k_2}^i\right)$$
$$=T_{2m}\left(\boldsymbol{q}^i,\boldsymbol{k}^i\right)-\beta_q^i\frac{\partial T_{2m}}{\partial \boldsymbol{q}^i}\boldsymbol{d}_q^i-\beta_{h_\infty}^i\frac{\partial T_{2m}}{\partial h_\infty^i}d_{h_\infty}^i-\beta_{k_S}^i\frac{\partial T_{2m}}{\partial k_S^i}d_{k_S}^i-\beta_{k_2}^i\frac{\partial T_{2m}}{\partial k_2^i}d_{k_2}^i \tag{18}$$

The term $\frac{\partial T_{2m}}{\partial \boldsymbol{q}^i}\boldsymbol{d}_q^i$ in the above equation can be replaced by $\Delta T_{\boldsymbol{q}m}^i\left(x_m,t;\boldsymbol{d}_{\boldsymbol{q}}^i\right)$, which is obtained by setting $\Delta\boldsymbol{q}^i=\boldsymbol{d}_{\boldsymbol{q}}^{\boldsymbol{i}}$ and then solving the sensitivity problem given by Eqs. (12-14) at the sensor location. Also the terms $\frac{\partial T_{2m}}{\partial \boldsymbol{k}^i}$ is determined by the finite difference approximation given by Eqs. (16). Calculating the direction of descent based on CGM (Eq. (8b)) requires determining the gradient directions for heat transfer coefficient and thermal conductivities.

By substituting Eq. (18) into Eq. (17) and differentiating the resulting expression with respect to $\left[\beta_q^i,\beta_{h_\infty}^i,\beta_{k_S}^i,\beta_{k_2}^i\right]$, the following set of linear equations is obtained for the search step sizes.

$$\begin{bmatrix} A_{q,q} & A_{q,h_\infty} & A_{q,k_S} & A_{q,k_2} \\ A_{h_\infty,q} & A_{h_\infty,h_\infty} & A_{h_\infty,k_S} & A_{h_\infty,k_2} \\ A_{k_S,q} & A_{k_S,h_\infty} & A_{k_S,k_S} & A_{k_S,k_2} \\ A_{k_2,q} & A_{k_2,h_\infty} & A_{k_2,k_S} & A_{k_2,k_2} \end{bmatrix}\begin{bmatrix} \beta_q^i \\ \beta_{h_\infty}^i \\ \beta_{k_S}^i \\ \beta_{k_2}^i \end{bmatrix}=\begin{bmatrix} B_q \\ B_{h_\infty} \\ B_{k_S} \\ B_{k_2} \end{bmatrix} \tag{19}$$

where

$$A_{p,p}=\sum_{m=1}^{M}\int_{t=0}^{t_f}\left[\Delta T_{pm}^i\left(y_m,t;\boldsymbol{d}_p^i\right)\right]^2 dt \tag{20a}$$

$$A_{p,g}=\sum_{m=1}^{M}\int_{t=0}^{t_f}\left[\Delta T_{pm}^i\left(y_m,t;\boldsymbol{d}_p^i\right)\Delta T_{gm}^i\left(y_m,t;\boldsymbol{d}_g^i\right)\right]dt \tag{20b}$$

$$B_p = \sum_{m=1}^{M} \int_{t=0}^{t_f} \left[\left(T_{2m}^i - Y_m^i \right) \Delta T_{pm}^i \left(y_m, t; \boldsymbol{d}_p^i \right) \right] dt \tag{20c}$$

In the above equation, p and g can be any of the unknown parameters.

Adjoint problem

In the iterative procedure of CGM for heat flux estimation, the direction of descent is dependent on the gradient of the objective function ($\nabla S\left[q^i(t) \right]$ in Eq. (8a)). The calculation of the gradient function is performed by solving the adjoint problem. Therefore, the adjoint problem must be derived. In this regard, the direct problem equations (Eqs. (1a) and (2a)) are first multiplied by Lagrange multiplier functions $\lambda_1(x,t)$ and $\lambda_2(x,t)$. Furthermore, the obtained equations are integrated over time and space domains of the problem. The resulting equations are added to the objective function given by Eq. (4) to obtain the following extended function:

$$\begin{aligned} S[\boldsymbol{P}] &= \sum_{m=1}^{M} \int_{t=0}^{t_f} \left[Y_m(t) - T_2(x_m, t; \boldsymbol{P}) \right]^2 dt \\ &+ \int_{t=0}^{t_f} \int_{x=0}^{d_{pcm}} \lambda_1(x,t) \left[\frac{\partial}{\partial t} \left(\rho_1 C p_1 T_1 + f \rho_1 L \right) - \frac{\partial}{\partial x} \left(k_1 \frac{\partial T_1}{\partial x} \right) \right] dx dt \\ &+ \int_{t=0}^{t_f} \int_{x=d_{pcm}}^{d_{pcm}+d_{brick}} \lambda_2(x,t) \left[\rho_2 C p_2 \frac{\partial T_2}{\partial t} - k_2 \frac{\partial^2 T_2}{\partial x^2} \right] dx dt \end{aligned} \tag{21}$$

The perturbed goal function $S_\varepsilon\left[q_\varepsilon(t) \right]$ in the direction of the perturbed $q_\varepsilon(t)$ is achieved by replacing $T_1(x,t)$ by $\left[T_1(x,t) + \varepsilon \Delta T_1(x,t) \right]$, $T_2(x,t)$ by $\left[T_2(x,t) + \varepsilon \Delta T_2(x,t) \right]$, $f(T_1)$ by $\left[f(T_1) + \varepsilon \Delta f(T_1) \right]$ and $q(t)$ by $\left[q(t) + \varepsilon \Delta q(t) \right]$. Then the variation $\Delta S\left[q(t) \right]$ can be derived by applying the following limiting process.

$$\Delta S\left[q(t)\right]=\lim_{\varepsilon\to 0}\frac{S_{\varepsilon}\left[q_{\varepsilon}(t)\right]-S\left[q(t)\right]}{\varepsilon} \tag{22}$$

which yields

$$\begin{aligned}\Delta S\left[q(t)\right]&=\int_{t=0}^{t_f}\int_{x=d_{pcm}}^{d_{pcm}+d_{brick}}2\sum_{m=1}^{M}\left\{\left[T_2\left(x_m,t;\boldsymbol{P}\right)-Y_m(t)\right]\Delta T_2(x,t)\,\delta\left(x-x_m\right)\right\}dxdt\\&+\int_{t=0}^{t_f}\int_{x=0}^{d_{pcm}}\lambda_1(x,t)\left[\frac{\partial\left(\bar{C}\Delta T_1\right)}{\partial t}-\frac{\partial^2\left(k_1\Delta T_1\right)}{\partial x^2}\right]dxdt\\&+\int_{t=0}^{t_f}\int_{x=d_{pcm}}^{d_{pcm}+d_{brick}}\lambda_2(x,t)\left[\rho_2 Cp_2\frac{\partial\Delta T_2}{\partial t}-k_2\frac{\partial^2\Delta T_2}{\partial x^2}\right]dxdt\end{aligned} \tag{23}$$

Performing integration by parts and utilizing initial and boundary conditions of the sensitivity problem, the following equation is obtained.

$$\begin{aligned}\Delta S\left[q(t)\right]&=\int_{t=0}^{t_f}\int_{x=d_{pcm}}^{D}\left\{\rho_2 Cp_2\frac{\partial\lambda_2}{\partial t}+k_2\frac{\partial^2\lambda_2}{\partial x^2}+2\sum_{m=1}^{M}\left\{\left[T_2\left(x_m,t;\boldsymbol{P}\right)-Y_m(t)\right]\delta\left(x-x_m\right)\right\}\right\}\Delta T_2(x,t)\,dxdt\\&+\int_{t=0}^{t_f}\int_{x=0}^{d_{pcm}}\left[\bar{C}\frac{\partial\lambda_1}{\partial t}+k_1\frac{\partial^2(\lambda_1)}{\partial x^2}\right]\Delta T_1(x,t)\,dxdt+\int_{t=0}^{t_f}\frac{\partial\lambda_1(0,t)}{\partial x}\Delta T_1(0,t)\,dt\\&-\int_{t=0}^{t_f}\left[k_2\frac{\partial\lambda_2(D,t)}{\partial x}+h_{\infty}\lambda_2(D,t)\right]\Delta T_2(D,t)\,dt\\&-\int_{t=0}^{t_f}\left[k_1\frac{\partial\lambda_1\left(d_{pcm},t\right)}{\partial x}-k_2\frac{\partial\lambda_2\left(d_{pcm},t\right)}{\partial x}\right]\Delta T_1\left(d_{pcm},t\right)dt\\&-\int_{x=0}^{d_{pcm}}\bar{C}\lambda_1\left(x,t_f\right)\Delta T_1\left(x,t_f\right)dx-\int_{x=d_{pcm}}^{D}\rho_2 Cp_2\lambda_2\left(x,t_f\right)\Delta T_2\left(x,t_f\right)dx\\&+\int_{t=0}^{t_f}\left[\lambda_1\left(d_{pcm},t\right)-\lambda_2\left(d_{pcm},t\right)\right]\frac{\partial\left[k_1\Delta T_1\left(d_{pcm},t\right)\right]}{\partial x}dt\\&+\int_{t=0}^{t_f}\lambda_1(0,t)\Delta q(t)\,dt\end{aligned} \tag{24}$$

Where $D\equiv d_{pcm}+d_{brick}$. If the first eight integrals on the right-hand side of Eq. (24), including $\Delta T_1(x,t)$ and $\Delta T_2(x,t)$, are allowed to vanish, the following final value problem for the Lagrange multiplier functions $\lambda_1(x,t)$ and $\lambda_2(x,t)$ is derived.

For the slag bath:

$$\bar{C}\frac{\partial \lambda_1}{\partial t} - k_1 \frac{\partial^2 \lambda_1}{\partial x^2} = 0; \quad 0 < x < d_{pcm} \text{ and } 0 < t \le t_f \tag{25a}$$

$$\frac{\partial \lambda_1}{\partial x} = 0; \quad x = 0 \text{ and } 0 < t \le t_f \tag{25b}$$

$$\lambda_1\left(x, t_f\right) = 0; \quad 0 < x < d_{pcm} \text{ and } t = t_f \tag{25c}$$

For the brick wall:

$$\rho_2 Cp_2 \frac{\partial \lambda_2}{\partial t} + k_2 \frac{\partial^2 \lambda_2}{\partial x^2} + 2\sum_{m=1}^{M}\left\{\left[T_2\left(x_m, t; \boldsymbol{P}\right) - Y_m\left(t\right)\right]\delta\left(x - x_m\right)\right\} = 0; \quad d_{pcm} < x < d_{pcm} + d_{brick} \text{ and } 0 < t \le t_f \tag{26a}$$

$$k_2 \frac{\partial \lambda_2}{\partial x} = -h_\infty \lambda_2; \quad x = \left(d_{pcm} + d_{brick}\right) \text{ and } 0 < t \le t_f \tag{26b}$$

$$\lambda_2\left(x, t_f\right) = 0; \quad d_{pcm} < x < d_{pcm} + d_{brick} \text{ and } t = t_f \tag{26c}$$

At the brick-slag interface:

$$k_1 \frac{\partial \lambda_1}{\partial x} = k_2 \frac{\partial \lambda_2}{\partial x}; \quad x = d_{pcm} \text{ and } 0 < t \le t_f \tag{27a}$$

where

$$\lambda_1\left(d_{pcm}, t\right) = \lambda_2\left(d_{pcm}, t\right); \tag{27b}$$

In the process of obtaining the above adjoint problem, the extended function given by Eq. (24) is reduced to the following equation.

$$\Delta S\left[q(t)\right] = \int_{t=0}^{t_f} \lambda_1(0,t)\,\Delta q(t)\,dt \tag{28}$$

By perturbing the heat flux function (given by Eq. (6)) and substituting the resulting functional in Eq. (28), the directional derivative of $S\left[q(t)\right]$ can be rewritten as:

$$\Delta S\left[q(t)\right] = \sum_{j=1}^{M}\left\{\int_{t=0}^{t_f} \lambda_1(0,t)\,B_j(t)\,dt\;\Delta q_j\right\} \tag{29}$$

By definition, the directional increment of the function $S\left[q(t)\right]$ can be expressed in the following general form:

$$\Delta S\left[q(t)\right] = \sum_{j=1}^{N}\left\{\nabla S\left[q(t)\right]\right\}_j \Delta q_j \tag{30}$$

A comparison of Eqs. (29) and (30) results in the following relation for the j^{th} component of the gradient vector $\nabla S\left[q(t)\right]$:

$$\left\{\nabla S\left[q(t)\right]\right\}_j = \int_{t=0}^{t_f} \lambda_1(0,t)\,B_j(t)\,dt \tag{31}$$

The gradient of objective function used in Eq. (8b) is computed by taking the derivative of Eq. (4) with respect to the unknown heat transfer and thermal conductivity coefficients, which yields:

$$\begin{bmatrix} \nabla S(h_\infty) \\ \nabla S(k_S) \\ \nabla S(k_2) \end{bmatrix} = \begin{bmatrix} -2\sum_{m=1}^{M}\int_{t=0}^{t_f}\left[Y_m(t) - T_2(x_m,t;\boldsymbol{P})\right]\dfrac{\partial T}{\partial h_\infty}\,dt \\ -2\sum_{m=1}^{M}\int_{t=0}^{t_f}\left[Y_m(t) - T_2(x_m,t;\boldsymbol{P})\right]\dfrac{\partial T}{\partial k_S}\,dt \\ -2\sum_{m=1}^{M}\int_{t=0}^{t_f}\left[Y_m(t) - T_2(x_m,t;\boldsymbol{P})\right]\dfrac{\partial T}{\partial k_2}\,dt \end{bmatrix} \tag{32}$$

Stopping criterion

During the iterative minimization of the objective function given by Eq. (4), large oscillations in the estimated parameters occur when the estimated temperatures approach the noisy measurements. So, the iterative process is stopped when the following discrepancy principle [18] is satisfied:

$$S\left[\boldsymbol{P}^{i+1}\right] < \varepsilon \tag{33}$$

For noise-free measurements, a minimal value is selected for ε. For the noisy measurements, the amount of tolerance, ε, is selected in such a way that the residuals between measured and estimated temperatures are of the same order of magnitude as the standard deviation of measurement errors, that is,

$$\varepsilon = M\sigma^2 t_f \tag{34}$$

where M and σ represent the number of sensors and standard deviation of the measurement errors, respectively.

Computational procedure

The step-by-step iterative procedure of the conjugate gradient method for solving the current non-linear inverse problem can be summarized as:

Step 1: Provide the vector of temperature measurements Y, initiate the vector of unknowns $\boldsymbol{P}^T = \left[h_\infty, k_S, k_2, q_0, q_1, q_2, ..., q_N\right]$, set $i=1$ and go to the next step.

Step 2: Knowing $\boldsymbol{P}^i$, Solve the direct problem given by Eqs. (1-3) and compute $T_1\left(x,t\right)$ and $T_2\left(x,t\right)$, then compute the objective function $S\left[\boldsymbol{P}^i\right]$ from Eq. (4).

Step 3: If the convergence criterion given by Eq. (33) is satisfied, stop the iterations. Otherwise, go to step 4

Step 4: Compute the Jacobian matrix ***J*** whose elements are presented in Eq. (16) for the perturbed unknown parameters.

Step 5: Knowing $T_1\left(x,t;\boldsymbol{P}^i\right)$, $T_2\left(x,t;\boldsymbol{P}^i\right)$ and $Y\left(x_m,t\right)$, solve the adjoint problem given by Eqs. (25-27) and compute $\lambda_1\left(0,t\right)$.

Step 6: Knowing $\lambda_1\left(0,t\right)$ and the Jacobian matrix ***J***, compute $\nabla S\left[q^i\left(t\right)\right]$ and $\begin{bmatrix}\nabla S\left(h_\infty\right)\\ \nabla S\left(k_S\right)\\ \nabla S\left(k_2\right)\end{bmatrix}^i$ from Eq. (31) and Eq.(32), respectively.

Step 7: Compute The conjugation coefficients γ_q^i, $\gamma_{h_\infty}^i$, γ_{k_S} and γ_{k_2} from Eq. (9).

Step 8: Compute both the vector of the descent direction $d_q^i\left(t\right)$ and $\begin{bmatrix}d_{h_\infty}\\ d_{k_S}\\ d_{k_2}\end{bmatrix}^i$ from Eq. (8).

Step 9: Set $\Delta q^i\left(t\right)=d_q^i\left(t\right)$ and solve the sensitivity problem given by Eqs. (12-14) to obtain $\Delta T_{\boldsymbol{q},m}^i\left(x_m,t;\boldsymbol{d}_q^i\right)$.

Step 10: Compute the search step sizes $\left[\beta_q^i,\beta_{h_\infty}^i,\beta_{k_S}^i,\beta_{k_2}^i\right]$ from Eqs. (19) and (20).

Step 11: Knowing the search step sizes $\left[\beta_q^i, \beta_{h_\infty}^i, \beta_{k_S}^i, \beta_{k_2}^i\right]$ and directions of descent $d_q^i(t)$ and $\begin{bmatrix} d_{h_\infty} \\ d_{k_S} \\ d_{k_2} \end{bmatrix}^i$, compute the new estimate of heat flux $q^{i+1}(t)$ and thermal parameters $\begin{bmatrix} h_\infty \\ k_S \\ k_2 \end{bmatrix}^{i+1}$ from Eq. (7). Replace *i* by *i+1* and return to step 2.

Once the heat flux $q(t)$ and the thermal parameters $\begin{bmatrix} h_\infty \\ k_S \\ k_2 \end{bmatrix}$ are estimated, the direct problem given by Eqs. (1-3) is solved to determine the time-varying bank thickness $\delta(t)$.

Inverse code verification and error analysis

The capability of the proposed inverse method in terms of stability and accuracy is evaluated in the current section. The performed verification and error analysis consist of four parts. In the first part, the performance of the proposed inverse method is evaluated for the noise-free inputs to assess the bias of the proposed estimator. Second, the effect of initial guesses considered for the unknowns on the convergence behavior of the proposed inverse method is evaluated. The two most important sources of error are the noisy measurements and misplacement of the sensors, which are discussed next. To evaluate the deviation of the estimated heat flux from its exact profile, the normalized Root-Mean-Square (RMS) error is defined as:

$$e_{RMS} = \sqrt{\frac{\int_0^{t_f} \left[q^{est}(t) - q^{ex}(t)\right]^2 dt}{\int_0^{t_f} \left[q^{ex}(t)\right]^2 dt}} \tag{35}$$

Case study

In the current case, the width of both PCM and brick walls is considered to be 0.5 m. The thermophysical properties of the brick wall and the slag are given in Table 2. It is considered that the right boundary condition is exposed to ambient temperature, T_∞, of 300 K and a convective heat transfer coefficient, h_∞, of 15 W/(m^2.K). The left boundary is exposed to the time-varying heat flux $q(t)$. In the current study, two different functions for $q(t)$, involving a sinusoidal variation and a double-step function, are considered as follows:

$$q(t) = 1.2\times10^4 + 9\times10^3 \sin^3\left(2\pi t / t_t\right) \tag{36a}$$

$$q(t) = \begin{cases} 0; & 0 \le t < 25000 \\ 2.4\times10^4; & 25000 \le t < 75000 \\ 0; & 75000 \le t < 125000 \\ 2.4\times10^4; & 125000 \le t < 175000 \\ 0; & 175000 \le t < 200000 \end{cases} \tag{36b}$$

where the total simulation time is $t_f = 2\times10^5\,(s)$.

The initial temperature of the furnace varies linearly between T_b and 300 K, which correspond to the left boundary of the slag and external surface of the brick wall, respectively. The left boundary temperature for the case involving sinusoidal heat flux is T_b=1450 K, and for the other case is T_b=1200 K. It is considered that the temperature measurements are taken by two sensors embedded inside the brick wall, i.e., x_1=0.5 m and x_2=0.9 m. Both sensors record data at the same frequency of 1 Hz, which corresponds to the grid points of the time-domain in the direct solution. The direct problem, as defined in section 3, is solved using the specified heat flux $q(t)$ to determine

the temperature field $T_1(x,t)$ and $T_2(x,t)$ inside the slag and the brick wall. The direct problem was solved by the finite volume method with a uniform grid of 4000 cells and a time step interval of 1s. The grid convergence study for all cases in the current paper showed that the results were not appreciably affected by further refining the grid or reducing the time step size. The calculations were done by a desktop with an Intel Core^{TM} i7-3632 processor and 8 GB RAM. On average, each iteration of the inverse solution, which includes direct, sensitivity and adjoint problems, takes 9 seconds.

Noise-free measurements

The time-varying heat flux in this test case has sinusoidal variation, as presented in Eq. (36a). The estimated heat flux and thermal parameters in the case of noise-free measurements are illustrated in Fig. 4 and Table 3. As illustrated in Fig. 4, there are some deviations between the estimated and exact profiles, especially in the initial and final times neighborhood. The gradient of the objective function is null at the final time of the simulation. Therefore, the initial guess used for the heat flux at final time is not altered during the iterative procedure of the conjugate gradient method. As seen in Fig. 4, the last 5 hours of estimation is affected by the null condition. In fact, for a simulated experiment with a duration of 55.5 hours, the estimated values in the final 5 hours are not reliable**.** This type of error can be removed by using either additional measurements or a shorter total time of interest.

The estimation error in the initial times is caused by the low thermal conductivity of the solid-phase PCM (k_S=4*W/(m.K)*), which is much lower than the thermal conductivity of liquid-phase PCM (k_L=20*W/(m.K)*). The solid thickness at initial time is 30cm, which is 60% of the total PCM material in the furnace. In fact, a significant volume of the furnace is occupied by the

insulating solid-phase PCM in the initial times. Therefore, the temperature sensitivity of the thermocouple to the heat flux has its lowest value in this time period. As time progresses, the melting process causes the volume of the solid-phase to decrease and replace it with a liquid-phase that has a higher thermal conductivity.

The errors associated with the estimation of thermal parameters, as given in Table 3, do not exceed 1.7%, which is quite reasonable. The predicted bank thickness is compared with the exact one in Fig. 5. Accordingly, the error of estimated bank thickness is within approximately ±2%, providing cogent evidence that the gradient functions are well determined in the inverse algorithm.

Effect of initial guess

The inverse problem is solved for three sets of the initial values given in Table 4. The convergence history diagrams for the unknown thermal parameters are illustrated in Fig. 6. The results reveal that the current iterative method provides reasonable convergence behavior for all parameters with different initial guesses. In case #3, the sensitivity of the temperatures to the unknown parameters and function in the neighborhood of the initial guesses was minimal. This ill-condition behavior of the problem caused large oscillations at the beginning of the iterations, resulting in instability of the estimation. In order to damp oscillations, the conventional iterative procedure of the CGM was equipped with an under-relaxation scheme. For this reason, the iterative process of case #3 converges more slowly than the other two cases, as can be seen in Fig. 6. The reduction of objective function versus iteration number for three cases is illustrated in Fig. 7.

Noisy measurements

One inevitable source of error concerns the presence of noise in temperature measurements of sensors. The noisy temperature measurements $Y^{noisy}(t)$ were obtained by perturbing the exact temperature values $Y^{exact}(t)$ by random errors having normal probability distribution with zero mean and standard deviation of σ, as follows:

$$Y^{noisy}(t) = Y^{exact}(t) + \omega\sigma \tag{37}$$

where parameter ω is a random variable that can take a value between -2.576 and 2.576 for the 99% confidence level. The standard deviation of error for the thermocouples that are usually used is in the range of [$0.01T_{max}$ - $0.05T_{max}$]. Accordingly, the standard deviation of $\sigma = 0.03T_{max}$ which is equal to $\sigma = 35K$ according to the temperature of the thermocouples, has been selected.

Two test cases involving sinusoidal and double-step variations for the heat load were selected to investigate the effect of random errors on the estimation results. The initial values for the double-step and sinusoidal heat flux were, respectively, set to 0 and 10,000 W/m^2. The rest of the parameters were initialized to the values of case #2 in section 5.3. Figures 8 and 9 illustrate the best-estimated heat flux in the presence of noise in measurements. It can be seen that the estimated heat flux with double-step variation is more affected by random errors than the sinusoidal one.

As another part of the results, the estimated thermal parameters are listed in Table 5. As expected, the error of parameters in the case with double-step heat flux is greater than the other one. Also, the errors associated with the external heat transfer coefficient are greater than those of the two parameters. The predicted bank thickness is compared with the exact profile for two test cases in Figs. 10 and 11. As shown, in most of the furnace operating time, the errors remain at the interval of ±5% for the problem with sinusoidal heat flux and ±10% for the other case. In the case of sinusoidal heat flux, the estimated bank thickness in the neighborhood of the final time is more

erroneous than that of other times. While in the latter case, the most discrepancies occur at the beginning and middle times. Figures 9 and 11 reveal that at pulse times of the heat flux (i.e., times when the heat flux suddenly rises or falls), the error of predicted bank thickness increases abruptly. Therefore, discontinuity in heat flux can be remarked as an important source of error. The reduction of objective function versus iteration number is illustrated in Fig. 12. The iterative procedure of CGM converges slower for the case involving double-step heat flux than for the sinusoidal one.

Misplacement of sensor

Another source of error in the estimation results is associated with the sensor misplacement. So, a 5 cm deviation was assumed from the exact position of the sensors (i.e., x_1=0.55m and x_2=0.85m). In this test case, the inverse problem was solved with noise-free measurements. The estimated heat flux for misplacement of TC1 and TC2 was compared with the original profile in Fig. 13. As can be seen, the installation error of the sensor located at the brick-slag interface (TC1) has a larger impact on the estimated heat flux. The evaluation of estimated thermal parameters given in Table 6 demonstrates that the estimation error caused by shifting TC1 is larger than TC2. Also, the thermal conductivity of solid PCM is less sensitive to such an error in sensor location than the other two parameters. The ratio of bank thickness error to the sensor misplacement error is illustrated in Fig. 14. It is found that the predicted bank thickness at early times of simulation is more sensitive to such an error in sensor junction, especially for the sensor embedded at the brick-slag interface.

Conclusion

A hybrid inverse method was developed to simultaneously estimate thermophysical parameters and boundary heat load in a smelting furnace. One of the advantages of the present method is low computational cost due to the use of adjoint method for gradient calculation. The validity of the proposed inverse formulation was done in two ways. First, the results obtained for the simulated errorless measurements were compared with exact profiles. Accordingly, the error of estimated bank thickness is approximately ±2%, providing convincing evidence that the gradient functions are well determined in the inverse algorithm. Second, it was shown that the iterative process could converge to the exact solution while starting from different initial guesses selected for the unknowns. Moreover, the effects of noisy measurements on the estimated bank front are evaluated. As reported in the result section, in most of the furnace operating time, the error of estimated bank remains at the interval of ±5% for the problem with sinusoidal heat flux and ±10% for the double step one. The results showed that if the installation location of TC1 has an error of 5cm, the estimated bank at early times can have an error of up to 3.3cm. While the bank error caused by the misplacement of TC1 reached a maximum of 1.7cm.

Nomenclature

A_1 , A_2	Coefficients defined by Eq. (20)
B_{11} , B_{22} , B_{12}	Coefficients defined by Eq. (20)
$\bar{C}$	A coefficient defined by Eq. (12d)
CGM	Conjugate Gradient Method
Cp	Heat capacity [J/kg K]
d	Direction of descent [Eq. (7)]
d_{brick}	Brick thickness [m]

d_{pcm}	PCM thickness [m]
f	Liquid fraction
h_{∞}	Heat transfer coefficient [W/(m^2.K)]
$\boldsymbol{J}$	Jacobian matrix [Eq.(15)]
k	Thermal conductivity [W/(m.K)]
L	Latent heat [J/kg]
LMM	Levenberg Marquardt Method
M	Number of sensors
N	Number of total time steps
$\boldsymbol{P}$	Vector of unknowns [Eq. (5)]
PCM	Phase Change Material
$q(t)$	Heat flux [W/m^2]
S	Objective function [Eq. (4)]
t	Time [s]
t_f	Final time [s]
T	Temperature [K]
T_{∞}	Ambient temperature [K]
x	Cartesian coordinate [m]
x_m	Sensor location [m]
Y	Sensor temperature [K]

Greek symbols

β	Step size [Eq. (7)]
γ	Conjugation coefficient [Eq. (9)]

$\delta(t)$	Bank thickness [m]
$\delta(x)$	Dirac delta function
ε	Small value
$\lambda(x,t)$	Lagrange multiplier [Eq. (17)]
ρ	Density [kg/m^3]
σ	Standard deviation [K]
$\Delta T(x,t)$	Sensitivity function
$\nabla S[\boldsymbol{P}]$	Gradient direction [defined by Eqs. (12-14)]

Subscripts

0	Initial condition
1	Slag region
2	Brick region
L	Liquid phase
S	Solid phase

superscript

T	Transpose of a matrix
i	Iteration index

REFERENCES

[1] Tadrari, O. and Lacroix, M., "Prediction of protective banks in high temperature smelting furnaces by inverse heat transfer", International journal of heat and mass transfer, 49(13-14), pp.2180-2189, (2006). https://doi.org/10.1016/j.ijheatmasstransfer.2005.11.023

[2] Su, C. R., "Geometry estimation of the furnace inner wall by an inverse approach", International Journal of Heat and Mass Transfer, 50(19-20), pp.3767-3773, (2007). https://doi.org/10.1016/j.ijheatmasstransfer.2007.02.024

[3] Su, C. R., "Inverse estimation for temperatures of outer surface and geometry of inner surface of furnace with two layer walls", Energy Conversion and Management, 49(2), pp.301-310, (2008). https://doi.org/10.1016/j.enconman.2007.06.010

[4] Buonomo, B., Ercole, D., Manca, O., et al., "Numerical analysis on a latent thermal energy storage system with phase change materials and aluminum foam," Heat Transfer Engineering, 41(12), pp. 1075-1084, (2020). https://doi.org/10.1080/01457632.2019.1600875

[5] Fornarelli, F., Camporeale, S. M., & Fortunato, B., "Convective effects in a latent heat thermal energy storage", Heat Transfer Engineering, 42(1), pp.1-22, (2021). https://doi.org/10.1080/01457632.2019.1685240

[6] Alexis, J., Ramirez, M., Trapaga, G., et al., "Modeling of a DC electric arc furnace heat transfer from the arc", ISIJ international, 40(11), pp. 1089-1097, 2000. DOI:10.2355/isijinternational.40.1089

[7] Liu, C. S., & Chang, J. R., "A homogenization method to solve inverse Cauchy–Stefan problems for recovering non-smooth moving boundary, heat flux and initial value" ,Inverse Problems in Science and Engineering, 29(13), pp.2772-2803, (2021). https://doi.org/10.1080/17415977.2021.1949591

[8] LeBreux, M., Désilets, M., & Lacroix, M., "Fast inverse prediction of phase change banks in high temperature furnaces with a Kalman filter coupled with a recursive least-square estimator", International journal of heat and mass transfer, 53(23-24), pp.5250-5260, (2010). https://doi.org/10.1016/j.ijheatmasstransfer.2010.07.034

[9] Marois, M. A., Désilets, M., & Lacroix, M., "Prediction of the bank formation in high temperature furnaces by a sequential inverse analysis with overlaps", Numerical Heat Transfer, Part A: Applications, 60(7), pp.561-579, (2011). https://doi.org/10.1080/10407782.2011.616777

[10] Marois, M. A., Désilets, M., & Lacroix, M., "Prediction of a 2-D solidification front in high temperature furnaces by an inverse analysis", Numerical Heat Transfer, Part A: Applications, 59(3), pp.151-166, (2011). https://doi.org/10.1080/10407782.2011.541220

[11] LeBreux, M., Désilets, M., & Lacroix, M., "Control of the ledge thickness in high-temperature metallurgical reactors using a virtual sensor", Inverse Problems in Science and Engineering, 20(8), pp.1215-1238, (2012).

https://doi.org/10.1080/17415977.2012.667090

[12] LeBreux, M., Desilets, M., & Lacroix, M., "An unscented Kalman filter inverse heat transfer method for the prediction of the ledge thickness inside high-temperature metallurgical reactors", International Journal of Heat and Mass Transfer, 57(1), pp.265-273, (2013).
https://doi.org/10.1016/j.ijheatmasstransfer.2012.10.036

[13] LeBreux, M., Desilets, M., & Lacroix, M., "Prediction of the time-varying ledge profile inside a high-temperature metallurgical reactor with an unscented Kalman filter-based virtual sensor," Numerical Heat Transfer, Part A: Applications, 64(7), pp. 551-576, (2013).
https://doi.org/10.1080/10407782.2013.790272

[14] Bertrand, C., Marois, M. A., Désilets, M., Soucy, G., & Lacroix, M., "A combined 2D inverse predictions and experimental analysis for the bank formation inside a metallurgical reactor", International Journal of Heat and Mass Transfer, 59, pp.58-65, (2013).
https://doi.org/10.1016/j.ijheatmasstransfer.2012.12.008

[15] Hafid, M., Lacroix, M., "An inverse heat transfer method for predicting the thermal characteristics of a molten material reactor", Applied Thermal Engineering, 108, pp.140-149, (2016).
https://doi.org/10.1016/j.applthermaleng.2016.07.087

[16] Farzan, H., Sarvari, S. H., & Mansouri, S. H., "Inverse boundary design of a radiative smelting furnace with ablative phase change phenomena", Applied Thermal Engineering, 98, pp.1140-1149, (2016).
https://doi.org/10.1016/j.applthermaleng.2016.01.029

[17] Hafid, M., Lacroix, M., "Inverse heat transfer prediction of the state of the brick wall of a melting furnace", Applied Thermal Engineering, 110, pp.265-274, (2017). https://doi.org/10.1016/j.applthermaleng.2016.08.162

[18] Hafid, M., Lacroix, M., "Inverse method for simultaneously estimating multi-parameters of heat flux and of temperature-dependent thermal conductivities inside melting furnaces", Applied Thermal Engineering, 141, pp.981-989, (2018). https://doi.org/10.1016/j.applthermaleng.2018.06.041

[19] Zhang, B., Mei, J., Zhang, C., et al., "A general method for predicting the bank thickness of a smelting furnace with phase change", Applied Thermal Engineering, 162, pp.114219, (2019). https://doi.org/10.1016/j.applthermaleng.2019.114219

[20] Zielonka, A., Hetmaniok, E., Słota, D., "Reconstruction of the boundary condition in the binary alloy solidification problem with the macrosegregation and the material shrinkage phenomena taken into account", Heat Transfer Engineering, 42(3-4), pp.308-318, (2021). https://doi.org/10.1080/01457632.2019.1699300

[21] Lv, C., Wang, G., Chen, H., et al., "Estimation of the moving heat source intensity using the multiple model adaptive inverse method", International Journal of Thermal Sciences, 138, pp.576-585, (2019). https://doi.org/10.1016/j.ijthermalsci.2019.01.018

[22] Wen, S., Qi, H., Ren, Y. T., et al., "Application of KF-RLSE algorithm for on-line estimating the time-dependent melting thickness and input heat flux in participating media", International Journal of Thermal Sciences, 125, pp.1-10, (2018). https://doi.org/10.1016/j.ijthermalsci.2017.11.008

[23] Devarani, N., & Joshi, S. N., "Determining alloyed layer thickness in electric discharge alloying by inverse estimation of energy distribution", International Journal of Thermal Sciences, 177, p.107571, (2022).
https://doi.org/10.1016/j.ijthermalsci.2022.107571

[24] Tahmasbi, V., Noori, S., "Inverse identification of temperature-dependent thermal conductivity coefficients in an orthotropic charring composite", Applied Thermal Engineering, 183, p.116219, (2021).
https://doi.org/10.1016/j.applthermaleng.2020.116219

[25] Gutiérrez, J. M., Aguado Teixe, J. M., Martín, J. A., et al., "A Hybrid Procedure for the Sequential Estimation of Surface Heat Flux From Measurements of Surface Temperature", Heat Transfer Engineering, 37(16), pp.1325-1340, (2016).
https://doi.org/10.1080/01457632.2016.1133987

[26] Tahmasbi, V., & Noori, S., "Application of Levenberg–Marquardt method for estimation of the thermophysical properties and thermal boundary conditions of decomposing materials", *Heat Transfer Engineering*, *41*(5), pp.449-475, (2020).
https://doi.org/10.1080/01457632.2018.1558010

[27] Niu, Z. T., Qi, H., Ji, Y. K., et al., "Real-time reconstruction of thermal boundary condition of porous media via temperature sequence", International Journal of Thermal Sciences, 177, p.107570, (2022).
https://doi.org/10.1016/j.ijthermalsci.2022.107570

[28] Courtois, E., Glouannec, P., Magueresse, A., et al., "Estimating thermal properties of phase change material from heat flux measurements", International Journal of Thermal Sciences, 172, p.107307, (2022).
https://doi.org/10.1016/j.ijthermalsci.2021.107307

[29] Wen, S., Qi, H., Yu, X. Y., et al., "Real-time estimation of time-dependent imposed heat flux in graded index media by KF-RLSE algorithm", Applied Thermal Engineering, 150, pp.1-10, (2019).
https://doi.org/10.1016/j.applthermaleng.2018.12.170

[30] Sun, S. "Simultaneous reconstruction of thermal boundary condition and physical properties of participating medium", International Journal of Thermal Sciences, 163, p.106853, (2021).
https://doi.org/10.1016/j.ijthermalsci.2021.106853

[31] Alibeyki, D., Mehryar, R., "Heat flux estimation in journal bearings using inverse heat transfer method", Heat and Mass Transfer, 57, pp.605-615, (2021).
https://doi.org/10.1007/s00231-020-02959-x

[32] Wei, L., Li, G., Song, M., et al., "Theoretical investigation on inverse identification of spectral properties of paraffin phase change materials based on multi-thickness model", Solar Energy, 225, pp.266-274, (2021).
https://doi.org/10.1016/j.solener.2021.07.006

[33] Tahmasbi, V., & Noori, S., "Extending Inverse Heat Conduction Method to Estimate Flight Trajectory of a Reentry Capsule", AUT Journal of Mechanical Engineering, 4(4), pp.505-522, (2020).
DOI: 10.22060/AJME.2020.17000.5845

[34] Sun, S., Chang, Z., Ji, Y., et al., "Inverse estimation of transient heat flux using sequential function specification method", Heat Transfer Engineering, 45(3), pp.233-243, (2024).
https://doi.org/10.1080/01457632.2023.2185488

[35] Sun, S., "Simultaneous reconstruction of thermal boundary condition and physical properties of participating medium", International Journal of Thermal Sciences, 163, p.106853, (2021).

https://doi.org/10.1016/j.ijthermalsci.2021.106853

[36] Beck, J. V., "Combined parameter and function estimation in heat transfer with application to contact conductance", Journal of heat transfer, 110(4b), pp. 1046-1058, (1988).

https://doi.org/10.1115/1.3250609

[37] Loulou, T., & Scott, E. P., "An inverse heat conduction problem with heat flux measurements", International Journal for Numerical Methods in Engineering, 67(11), pp.1587-1616, (2006).

https://doi.org/10.1002/nme.1674

[38] Loulou, T., "Combined parameter and function estimation with application to thermal conductivity and surface heat flux", Journal of heat transfer, 129(10), pp.1309-1320, (2007).

https://doi.org/10.1115/1.2755064

[39] Molavi, H., Hakkaki-Fard, A., Rahmani, R. K., et al., "A novel methodology for combined parameter and function estimation problems", Journal of heat transfer, 132(12), p.121301, (2010).

https://doi.org/10.1115/1.4002283

[40] Ma, T., & Lavers, J., "A finite element iterative simulation of coupled electrothermal effects in an electric smelting furnace", IEEE Transactions on Magnetics, 21(6), pp.2416-2419, (1985).

DOI: 10.1109/TMAG.1985.1064219

[41] Voller, V. R., Swaminathan, C. R., "General Source-based method for solidification phase change", Numerical Heat Transfer, Part B Fundamentals, 19(2), pp.175-189, (1991). https://doi.org/10.1080/10407799108944962

Biography

Vahid Tahmasbi received his Ph.D. degree in aerospace engineering from Amirkabir University of Technology, Tehran, Iran, in 2020. He is working as a lecturer at Amirkabir University of Technology. His research activity is in the fields of aerodynamic heating and inverse heat conduction problems.

S. M. Hossein Karimian is professor at Amirkabir University of Technology. He received his Ph.D. in Mechanical Engineering from University of Waterloo in 1994, and attended Amirkabir University in 1995. His current research interests are heat transfer, vertical axis wind turbines, and fluid flows with dynamic stall.

Sahar Noori is an associate professor at Amirkabir University of Technology, Tehran, Iran. She received her Ph.D. degree in 2007, in aerodynamics, from Amirkabir University of Technology, Tehran, Iran. She is currently working on conduction and radiation heat transfer and inverse problems.

Table 1 properties of the binary Al-4.5% Cu alloy

Parameter	**Value**	**Unit**
Cp_S	900	[J/kg K]
k_S	200	[W/(m.K)]
$\rho_S \left(= \rho_L\right)$	2800	[Kg/m^3]
Cp_L	1100	[J/kg K]
K_L	90	[W/(m.K)]
L	3.9×10^5	[J/kg]
T_S	821	[K]
T_L	919	[K]

Table 2 Thermophysical properties of the phase change material and brick.

parameter	Value	Unit
PCM		
$Cp_S = Cp_L$	1800	[J/kg K]
k_S	4	[W/(m.K)]
ρ_S	2100	[Kg/m^3]
ρ_L	2000	[Kg/m^3]
k_L	20	[W/(m.K)]
L	5.1×10^5	[J/kg]
T_S	1213	[K]
T_L	1233	[K]
Brick		
Cp	875	[J/kg K]
k	16.8	[W/(m.K)]
ρ	2600	[Kg/m^3]

Table 3 Estimated thermal parameters for the case with sinusoidal heat flux and noise-free measurements.

		Free noise measurements	
Parameter	**Exact value**	**Estimated**	**Error (%)**
$k_2\left[W/\left(m.k\right)\right]$	16.8	16.64	0.9
$k_S\left[W/\left(m.k\right)\right]$	4.0	3.93	1.7
$h_\infty\left[W/\left(m^2.k\right)\right]$	15.0	14.83	1.1

Table 4 Different initial values used for the validation of the inverse problem.

Unknown	Exact values	Initial guess		
		Case #1	Case #2	Case #3
Brick conductivity, $k_2\left[W/\left(m.k\right)\right]$	16.8	5.0	5.0	30.0
Bank conductivity, $k_S\left[W/\left(m.k\right)\right]$	4.0	15.0	1.0	20.0
Heat transfer coef., $h_\infty\left[W/\left(m^2.k\right)\right]$	15.0	30.0	40.0	5.0
Heat flux, $q\left(t\right)\left[kW/m^2\right]$	Eq. (31a)	5000.0	10000.0	10000.0

Table 5 Estimated thermal parameters from noisy measurements with $\sigma = 35K$.

Parameter	Exact value	Noisy measurements	
		Estimated	Error (%)
Sinusoidal heat flux case			
$k_2\left[W/(m.k)\right]$	16.8	16.04	4.5
$k_S\left[W/(m.k)\right]$	4.0	3.81	4.7
$h_\infty\left[W/(m^2.k)\right]$	15.0	14.18	5.4
Step heat flux case			
$k_2\left[W/(m.k)\right]$	16.8	18.36	9.2
$k_S\left[W/(m.k)\right]$	4.0	4.30	7.5
$h_\infty\left[W/(m^2.k)\right]$	15.0	16.88	12.5

Table 6 Effect of sensor misplacement on the estimated thermal parameters for noise-free measurements.

Parameter	Exact value	TC1		TC2	
		Estimated	Error (%)	Estimated	Error (%)
$k_2\left[W/\left(m.k\right)\right]$	16.8	14.72	12.3	15.0	10.7
$k_S\left[W/\left(m.k\right)\right]$	4.0	4.98	24.5	3.67	8.2
$h_\infty\left[W/\left(m^2.k\right)\right]$	15.0	15.43	2.8	16.35	9.0

List of Figure Captions

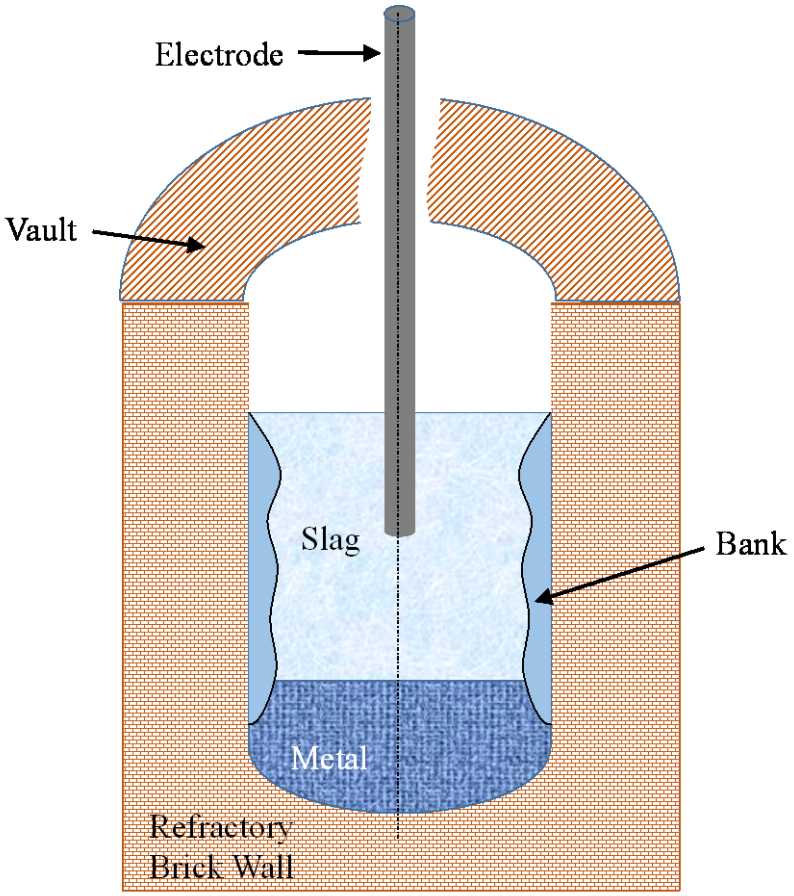

Figure 1 Schematic view of a smelting furnace.

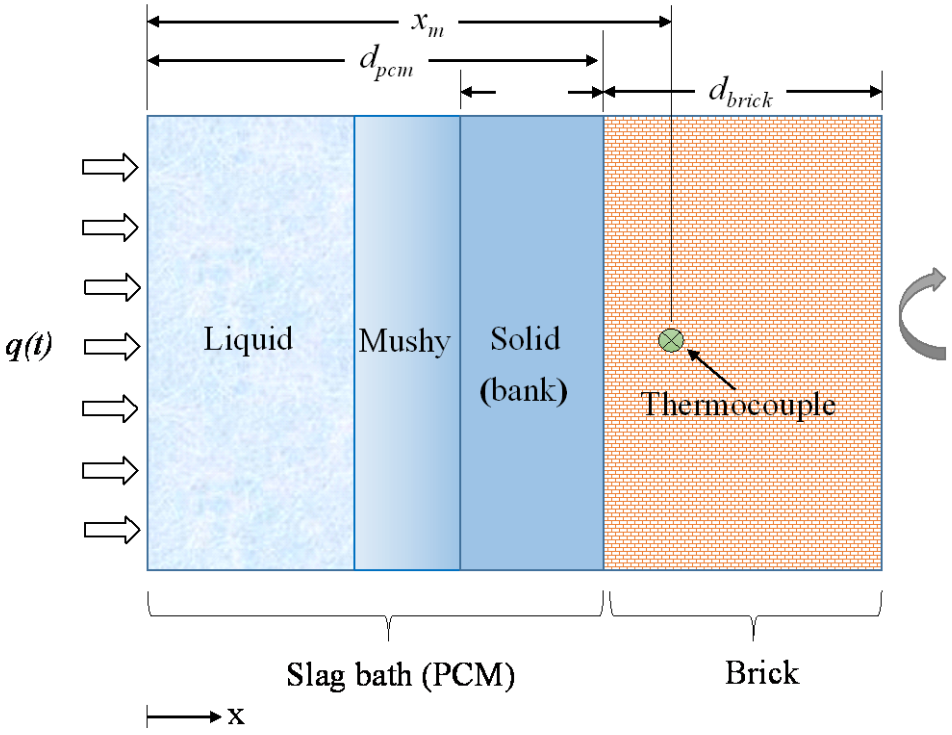

Figure 2 One dimensional model of the melting furnace with slag bath and brick wall.

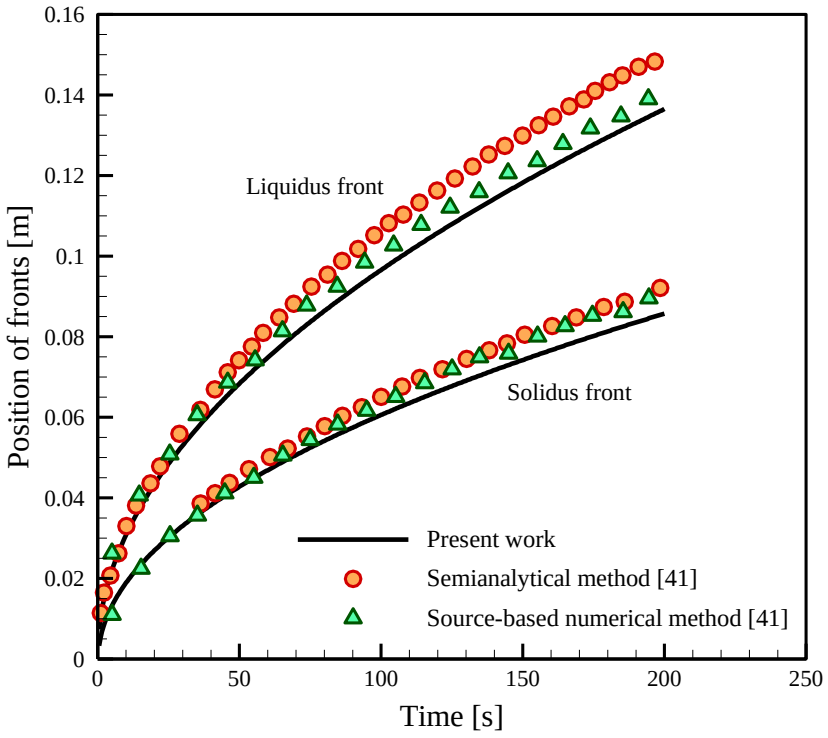

Figure 3 solidus and liquidus fronts for solidification of a binary Al-4.5% Cu alloy.

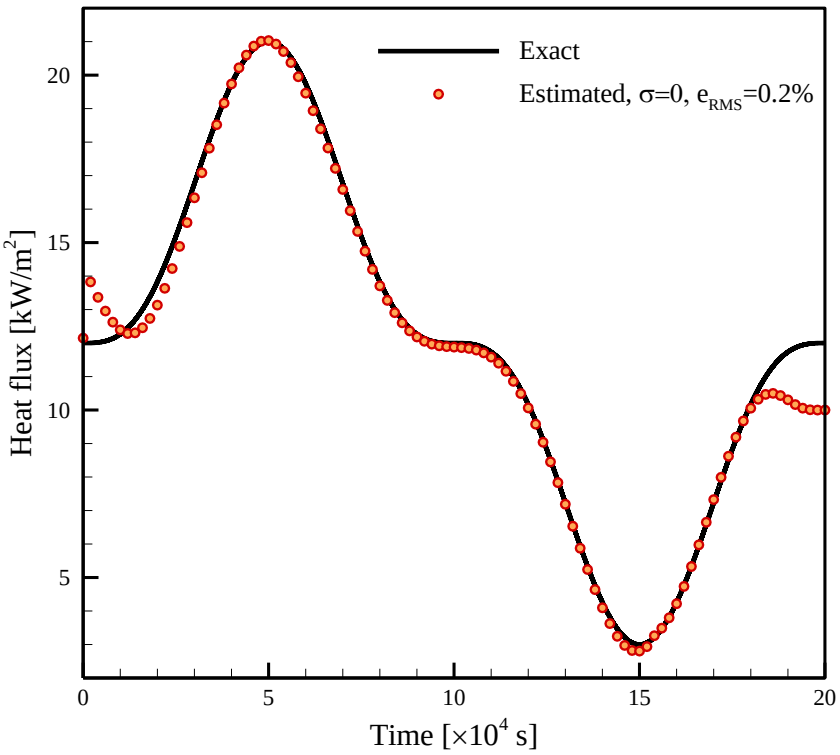

Figure 4 Inverse solution with sinusoidal variation for the heat flux and noise-free measurements.

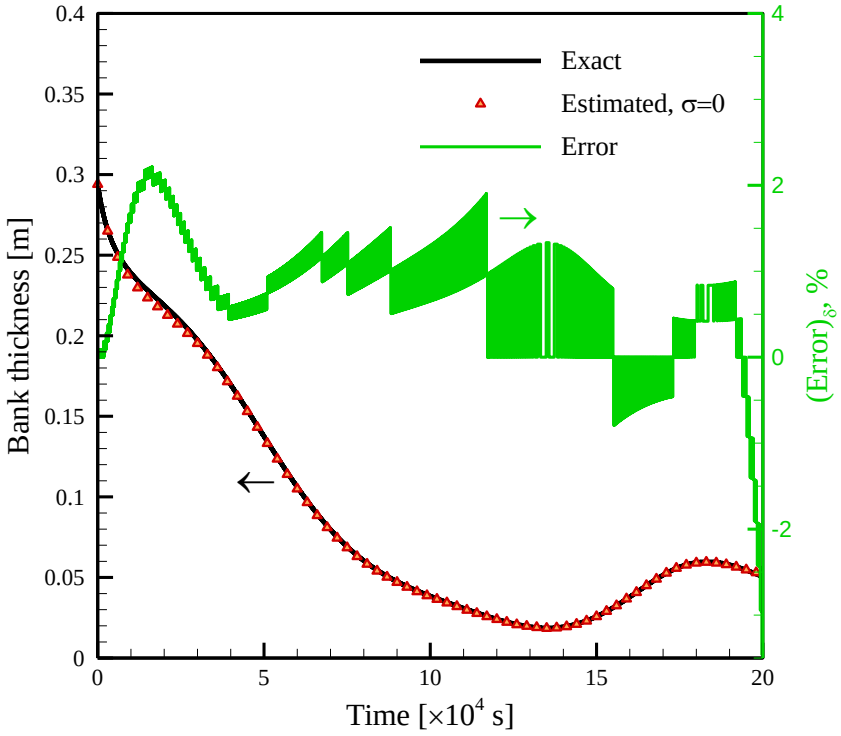

Figure 5 Predicted bank thickness for the sinusoidal heat flux and noise-free measurements.

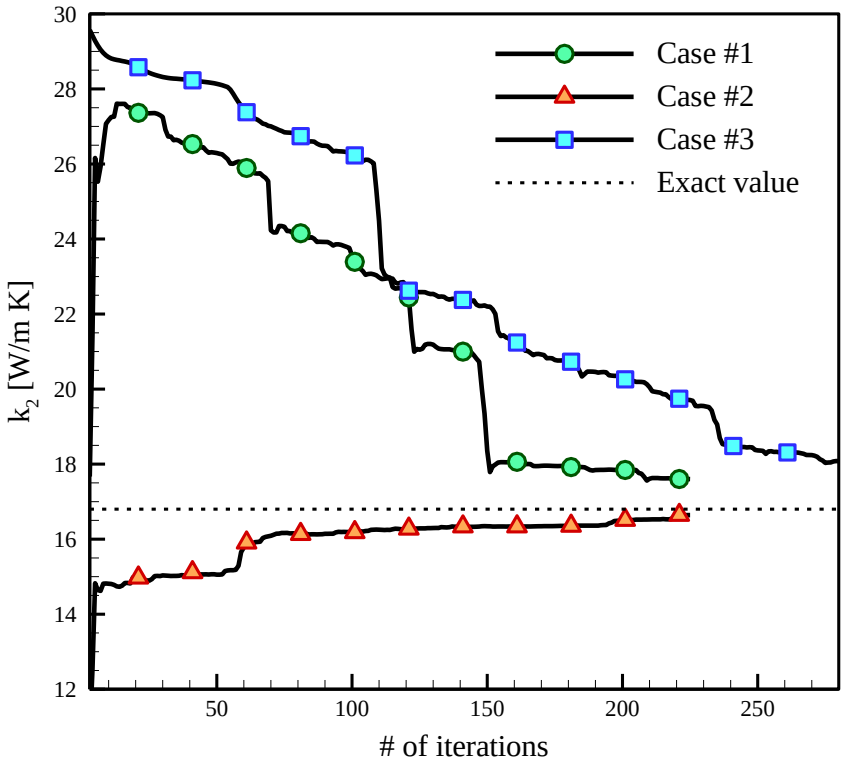
Case #1
Case #2
Case #3
Exact value
k2 [W/m K]
# of iterations
30
28
26
24
22
20
18
16
14
12
50
100
150
200
250

(a)

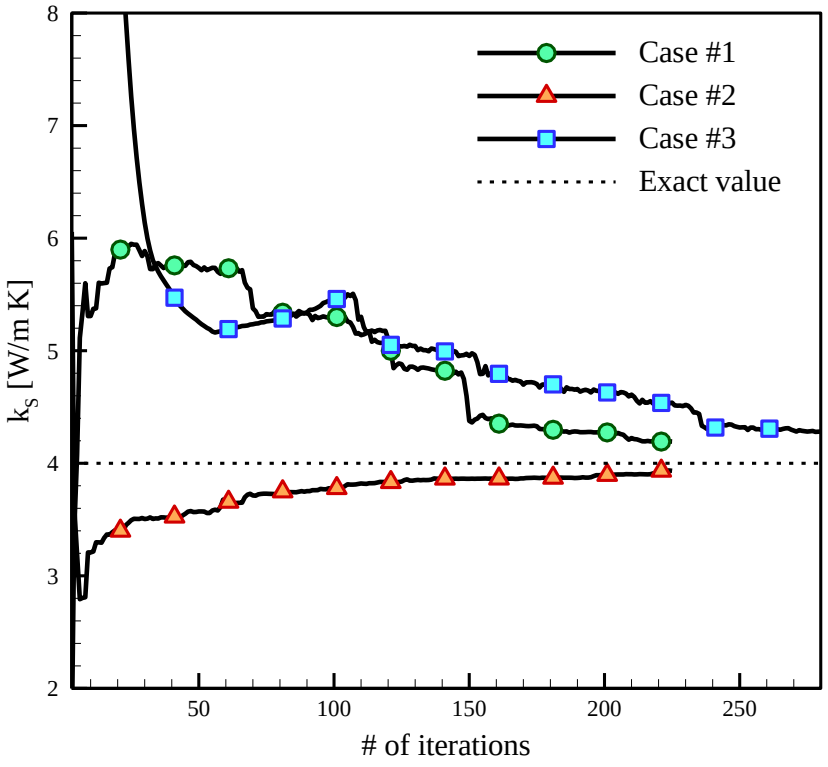
Case #1
Case #2
Case #3
Exact value
ks [W/m K]
# of iterations
8
7
6
5
4
3
2
50
100
150
200
250

(b)

Figure 6 (continued)

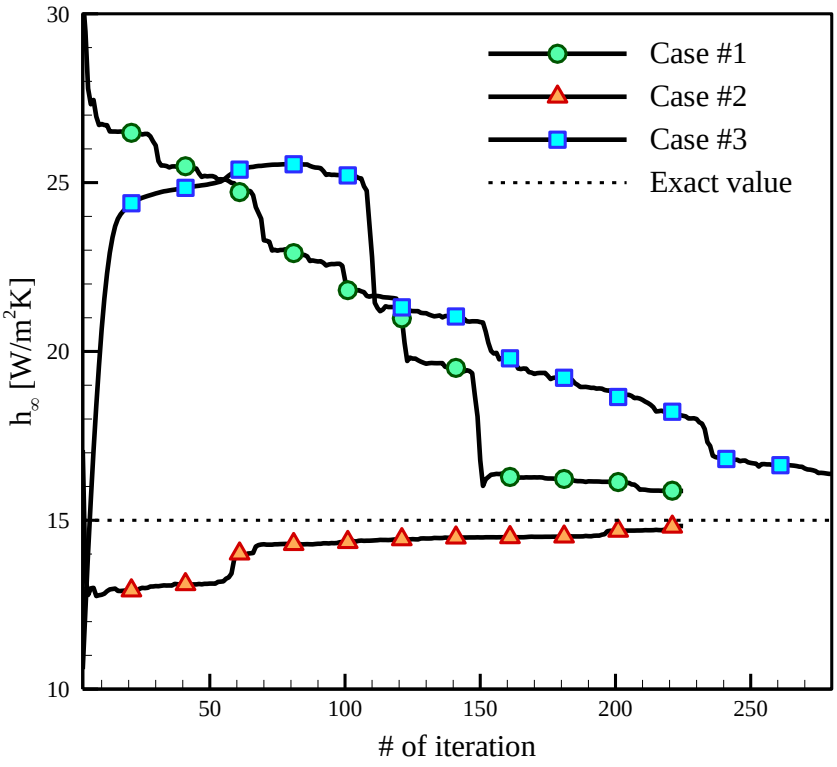

(c)

Figure 6 Convergence history of thermal parameters for different initial guesses and noise-free measurements for (a) brick wall conductivity, (b) solid PCM conductivity, and (c) external heat transfer coefficients.

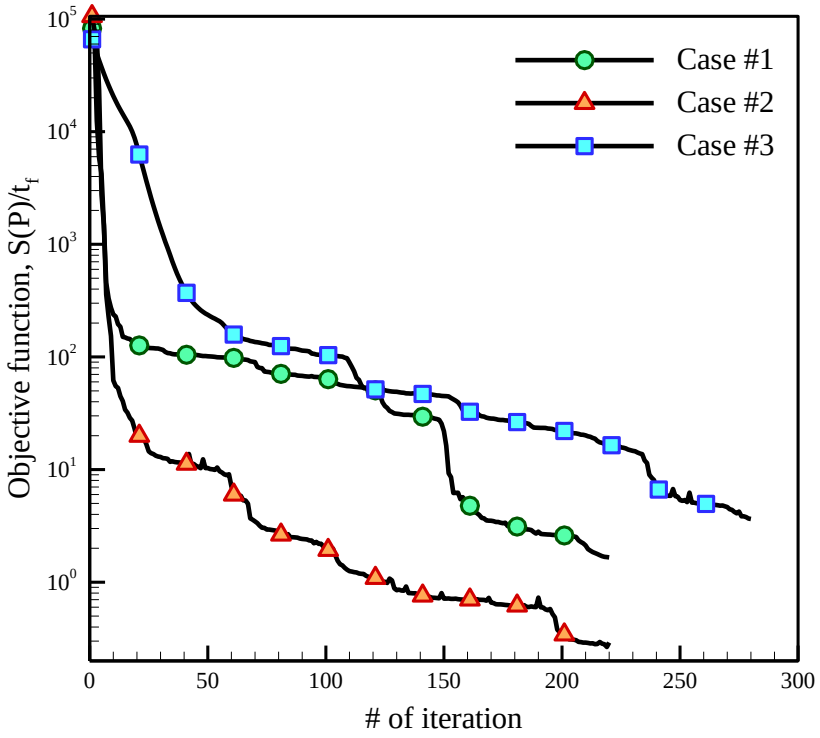

Figure 7 The value of objective function versus iteration number for the problems with different initial guesses.

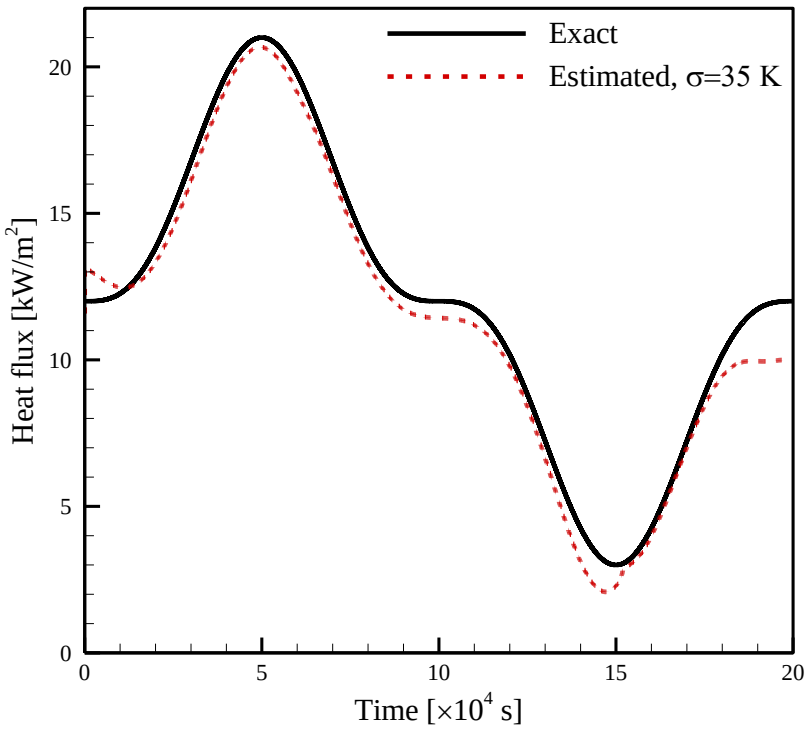

Figure 8 Estimated sinusoidal heat flux compared with exact profile for noisy measurements with $\sigma = 35K$.

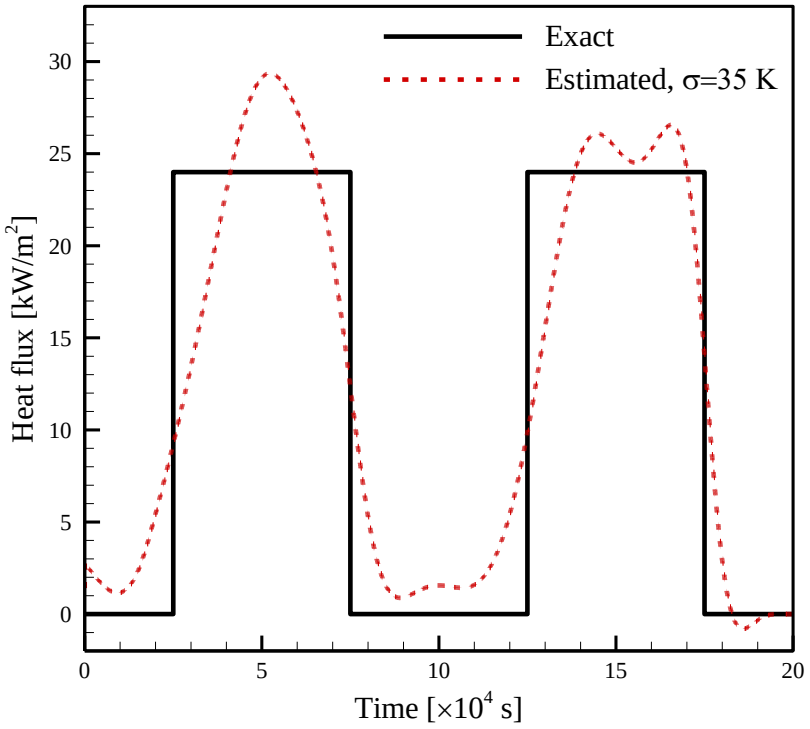

Figure 9 Estimated step heat flux compared with exact profile for noisy measurements with $\sigma = 35K$.

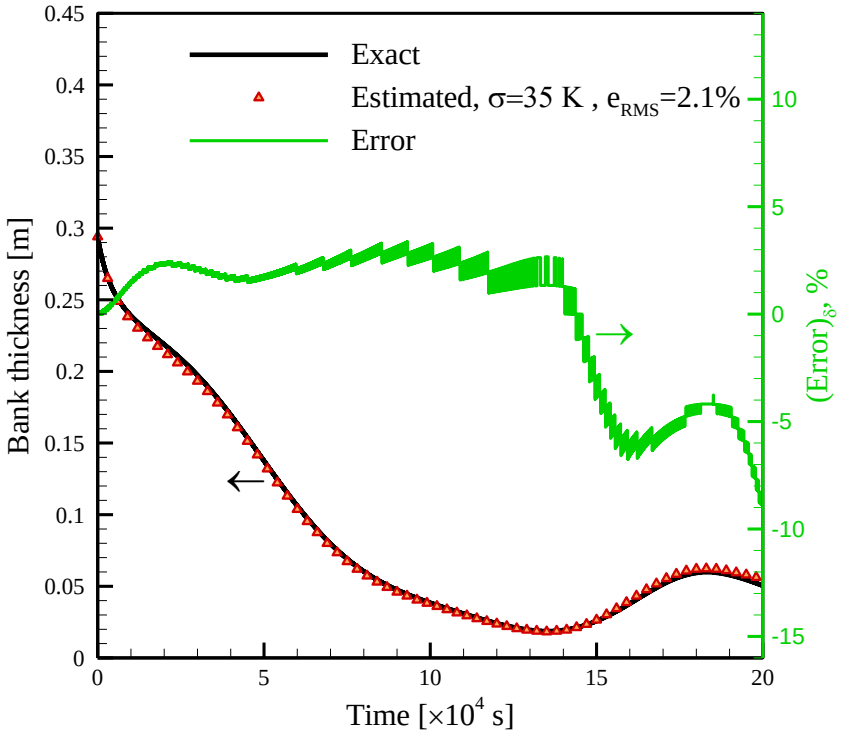

Figure 10 Comparison of estimated bank thickness with the exact profile for sinusoidal boundary heat flux and noisy measurements with $\sigma = 35K$.

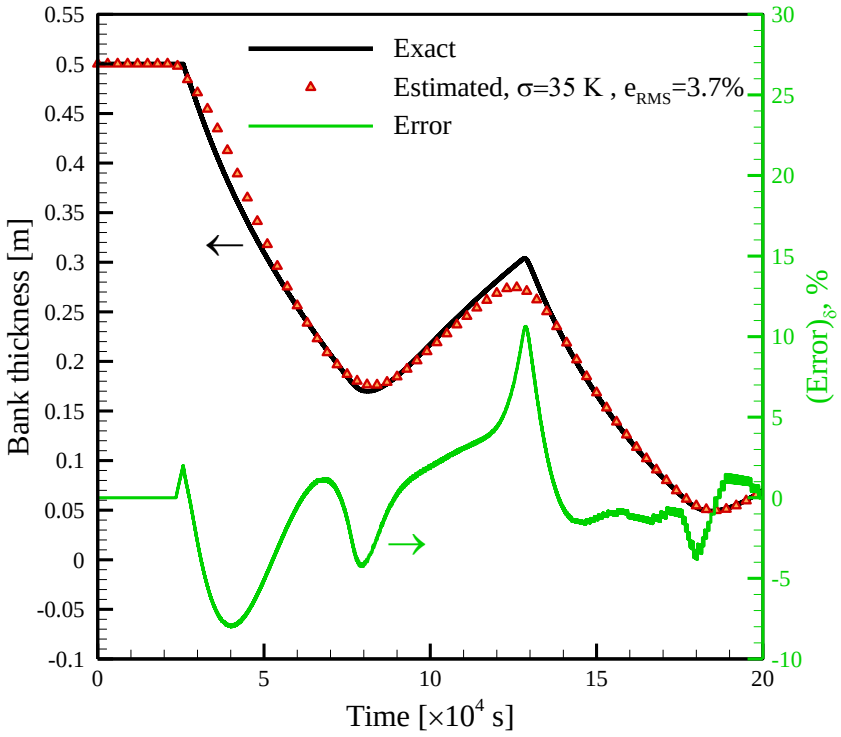

Figure 11 Comparison of estimated bank thickness with the exact profile for step boundary heat flux and noisy measurements with $\sigma = 35K$.

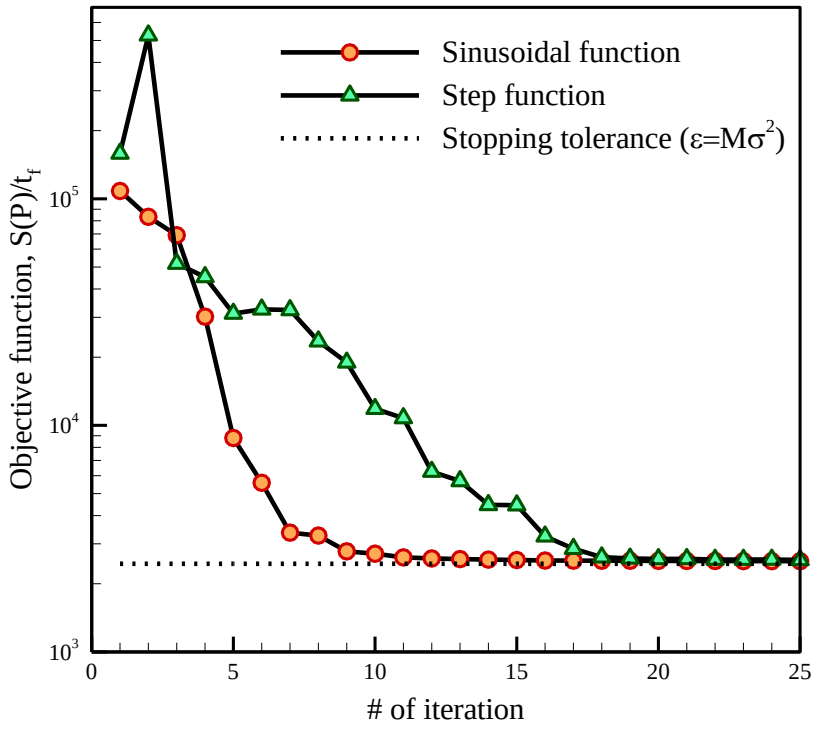

Figure 12 The objective function value versus iteration number for noisy measurements with $\sigma = 35K$.

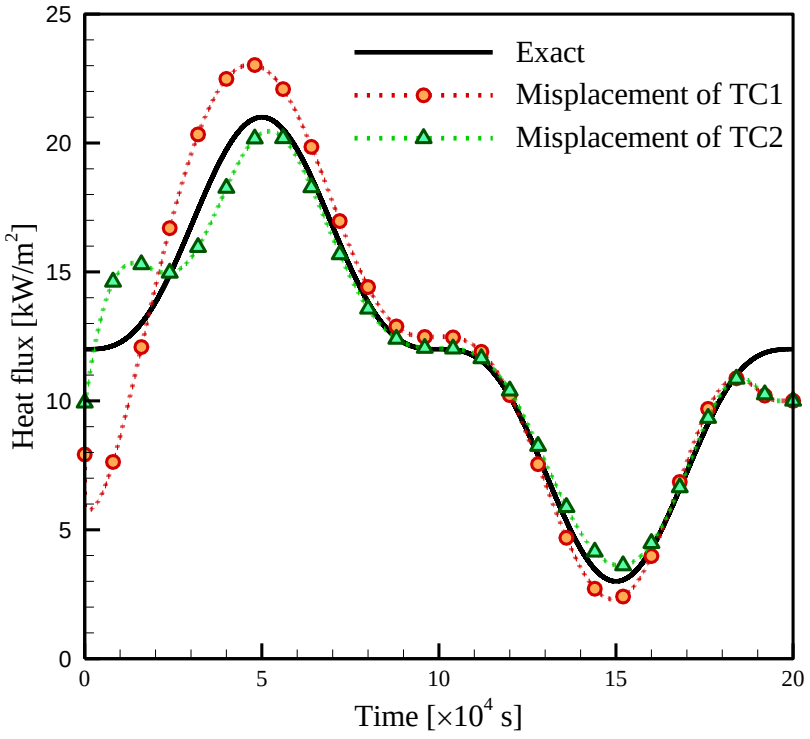

Figure 13 Effect of sensor misplacement on the estimated heat flux for noise-free measurements.

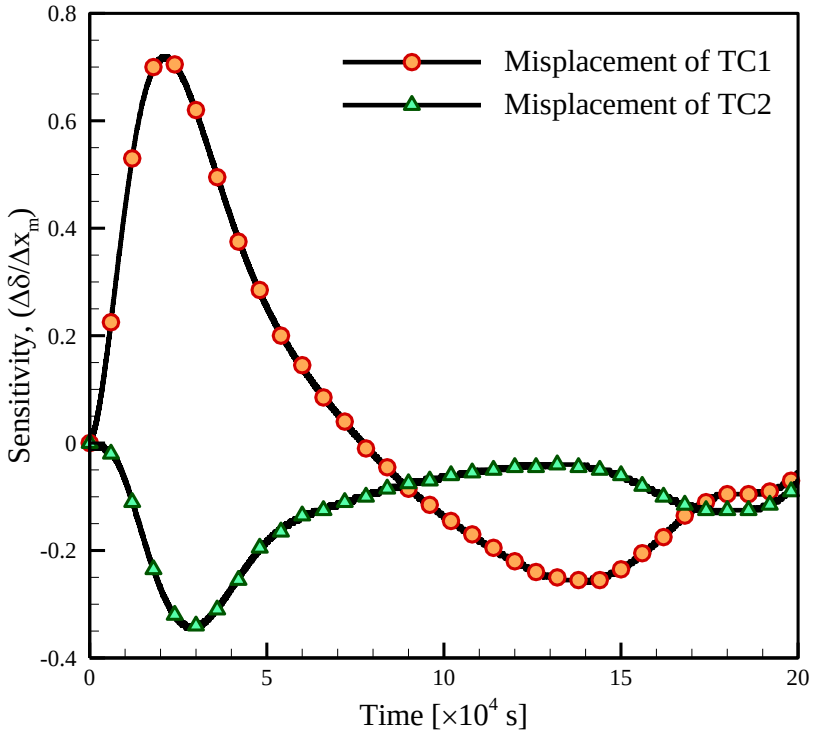

Figure 14 Effect of sensor misplacement on the predicted bank thickness for noise-free measurements.